Appendix 1

The reason why DECT was applied in patients with PTC

The success of surgery for thyroid cancer hinges on thorough and accurate preoperative imaging, which enables complete clearance of the primary tumor and affected lymph node compartments. Although US is a standard modality for the assessment of cervical LNM in patients with thyroid cancer, there has been an increasing trend in the number of articles describing the use of contrast-enhanced CT. We searched multiple databases, including PubMed, Web of Science, and Medline, using "CT" and "thyroid cancer" as keywords, and retrieved 16 relevant studies from the past 5 years (18,34,35,43-45). The value of CT examination in patients with thyroid cancer has been evidenced by these studies.

The literature cited by many articles on the application of DECT in the diagnosis of PTC and cervical LNM was published in Radiology in 2015 (34); this study has been cited many times in recent years. This reference evaluated the use of DECT quantitative parameters compared with the use of conventional CT imaging features for the preoperative diagnosis of metastasis of the cervical lymph nodes in patients with PTC. The results showed that DECT quantitative parameters had higher accuracy than the qualitative assessment of conventional CT imaging features for preoperative diagnosis of metastatic cervical lymph nodes in patients with PTC.

Besides, a systematic review and meta-analysis published in European Radiology in 2019 studied the diagnostic performance of contrast-enhanced CT, and the results showed that CT demonstrated an acceptable diagnostic performance in the pre- and postoperative diagnosis of metastatic cervical LNs in patients with thyroid cancer (45).

We have listed only two classic references above. The other 14 references also support the value of CT in the

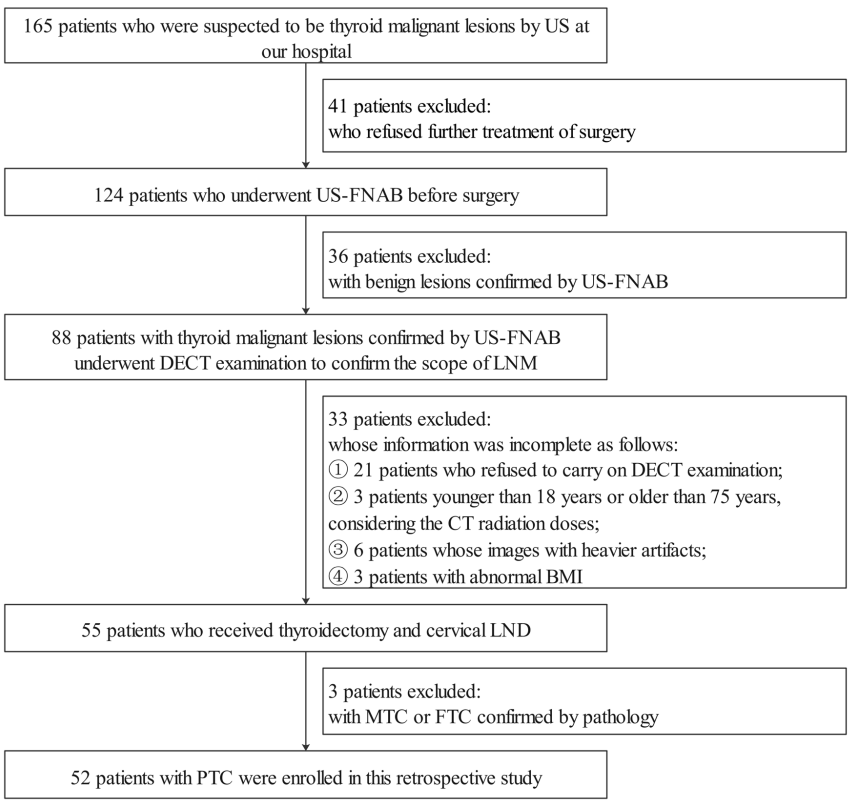

Figure S1 Flowchart showing criteria of inclusion and exclusion for patients with PTC. US, ultrasound; US-FNAB, ultrasound-guided fine needle aspiration biopsy; DECT, dual-energy computed tomography; LNM, lymph node metastasis; BMI, body mass index; LND, lymph node dissection; MTC, medullary thyroid carcinoma; FTC, follicular thyroid carcinoma; PTC, papillary thyroid carcinoma.

http://dx.doi.org/10.21037/qims-20-846

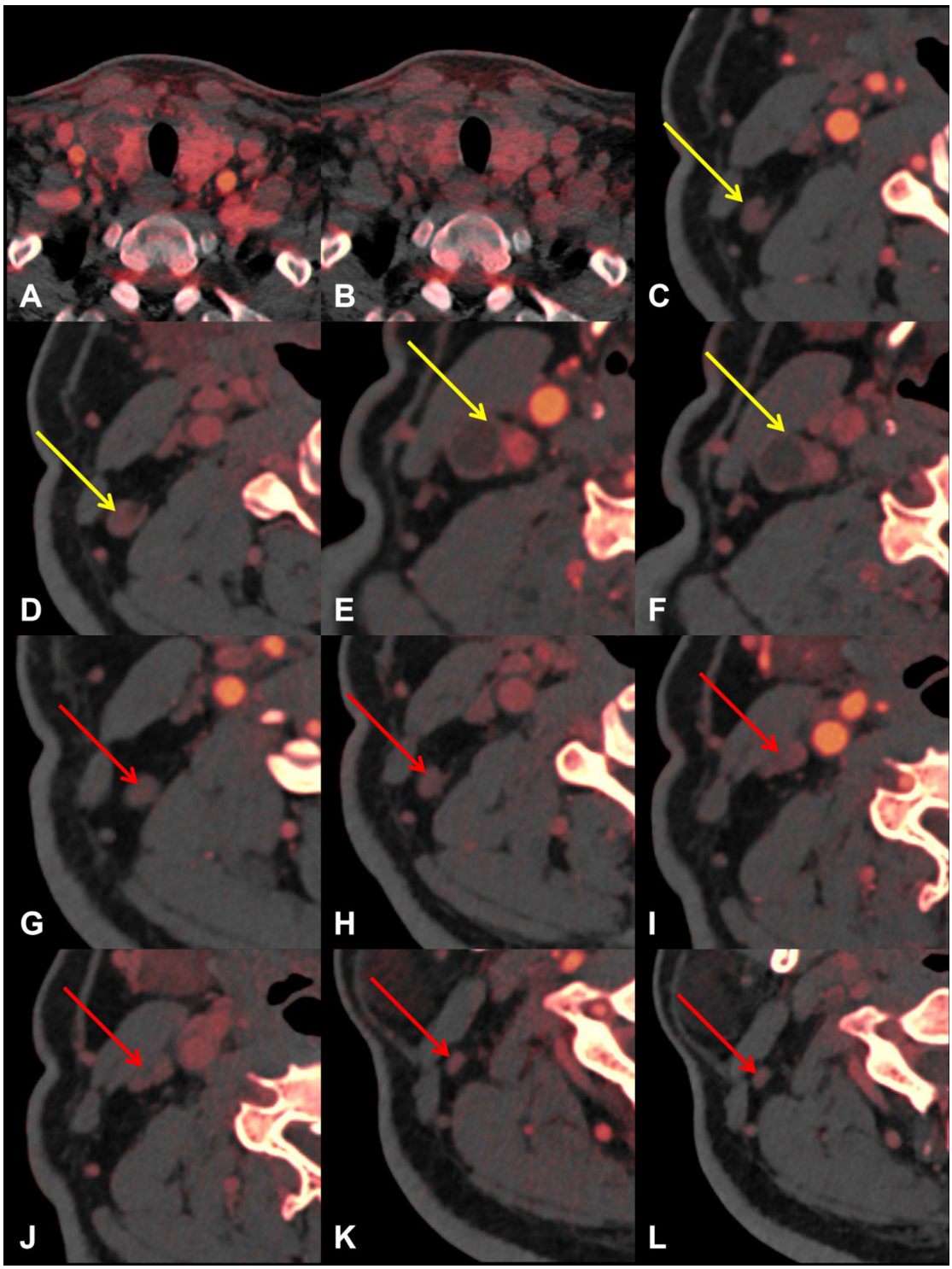

Figure S2 An example in which one level is full of metastatic LNs. Male, 30 years old, total thyroidectomy accompanied by bilateral neck LN dissection. Postoperative pathological results showed that diffuse PTC and LN metastasis in right level II (5/5). (A,B) Arterial and venous iodine maps of primary lesions; (C,D,E,F) two LNs with a short diameter ≥0.5 cm (yellow arrow); (G,H,I,J,K,L) another three LNs with short diameter <0.5 cm (red arrow). We only included three LNs <0.5 cm, and two LNs ≥0.5 cm was excluded. PTC, papillary thyroid carcinoma; LN, lymph node.

http://dx.doi.org/10.21037/qims-20-846

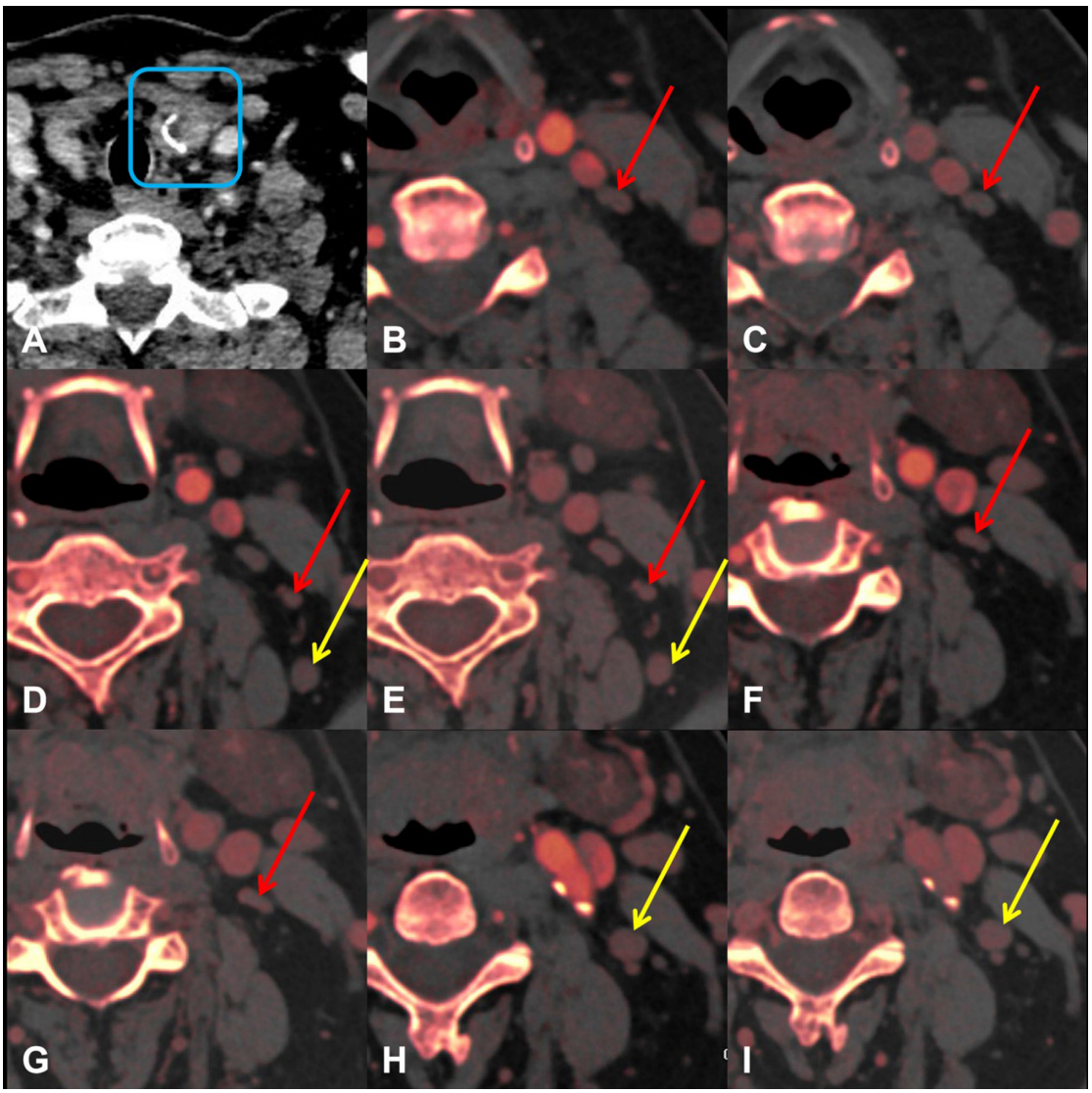

Figure S3 Another example in which one level is full of non-metastatic LNs. Female, 59 years old, left thyroid lobectomy accompanied with left cervical LN dissection. Postoperative pathological results showed that the left thyroid lobe was considered to be papillary thyroid microcarcinoma with calcification. There were no metastatic LNs in the left level II (0/5). (A) Arterial phase image of the primary tumor (blue square); (B-H) three LNs with short diameter <0.5 cm (red arrow) in the arterial and venous phases. (E-I) Another two LNs with a short diameter ≥0.5 cm (yellow arrow) in the arterial and venous phases. We only included three LNs <0.5 cm, and two lymph nodes ≥0.5 cm were excluded. LN, lymph node.

http://dx.doi.org/10.21037/qims-20-846

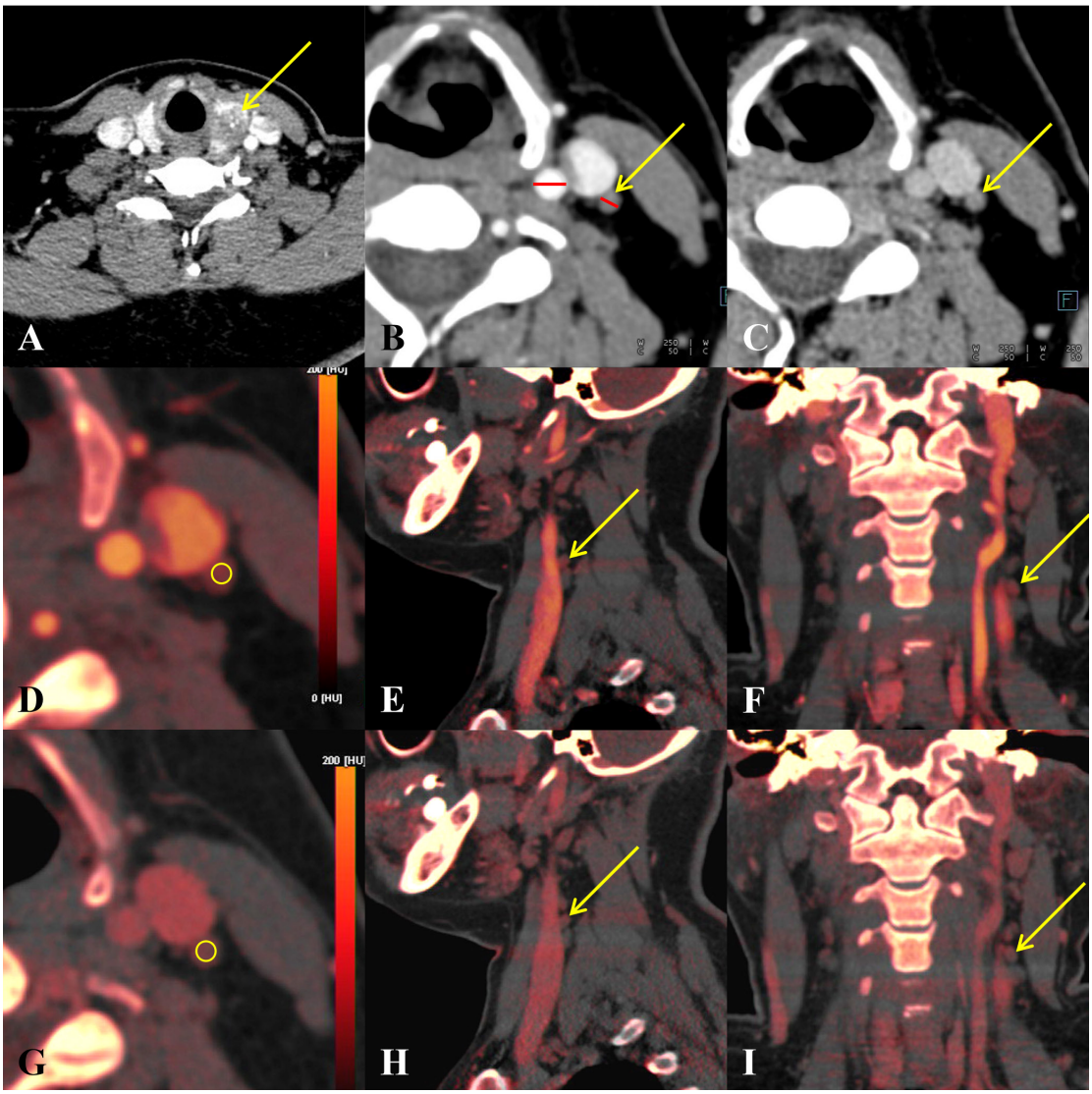

Figure S4 Illustration of specific methods for IC measurement. Female, 36 years old, total thyroidectomy and cervical LN dissection were performed. Pathology confirmed PTC of left lobe with a diameter 1.7 cm (A) all three lymph nodes in the left level IV were metastatic. We measured one of the LNs (diameter of 0.35 cm) as an example. First, by observing the original images of the selected LN in the arterial and venous phases (B,C), it was determined that the lesion contained enough solid parts to be measured excluding cystic degeneration, necrosis, or calcification. Then, we found the corresponding LN on the iodine map. Under the premise of ensuring sufficient clear resolution, the LN was enlarged in the axial images (D,G), and the ROI was placed on the solid part of the lesion during measurement, excluding cystic degeneration, necrosis, or calcification, and ensuring that it did not include adjacent blood vessels. We comprehensively observed the axial, sagittal (E,H), and coronal (F,I) directions to ensure the accuracy of the measurement. For comparison, the diameter of the common carotid artery on the same plane that was simultaneously measured was 0.7 cm (B). IC, iodine concentration; ROI, region of interest; LN, lymph node; PTC, papillary thyroid carcinoma.

http://dx.doi.org/10.21037/qims-20-846

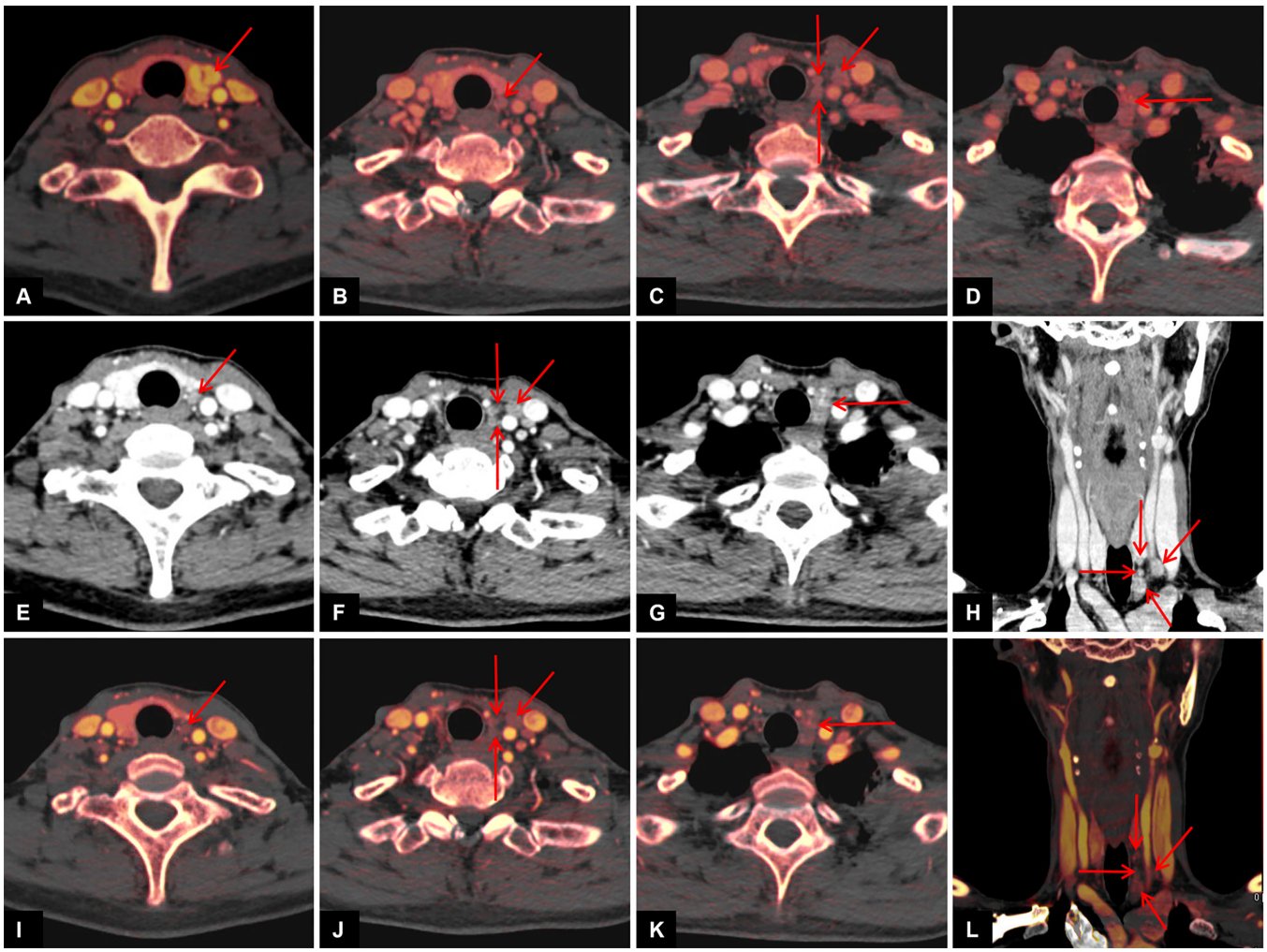

Figure S5 An example of pathological results and DECT both showing that all metastatic lymph nodes are in 1 level. Female, 52 years old. Left lobe and left level VI dissection were performed. Pathology confirmed PTC of the left lobe with a diameter 1.1 cm (A) and five metastatic LNs were found in the left level VIb. From the DECT images, we also found five metastatic LNs in the left level VIb in the iodine map in the arterial phase (red arrow, B-D) and on contrast-enhanced arterial phase (red arrow, E-H), the ICs of these metastatic LNs were 4.2, 3.1, 3.3, 3.2, and 4.4 mg/mL, respectively. In the venous phase, the ICs of these five metastatic LNs were 4.5, 3.4, 3.1 mg/mL, 3.1, and 3.7 mg/mg, respectively (red arrow, I-L). DECT, dual-energy computed tomography; IC, iodine concentration; PTC, papillary thyroid carcinoma; Ln, lymph node.

http://dx.doi.org/10.21037/qims-20-846

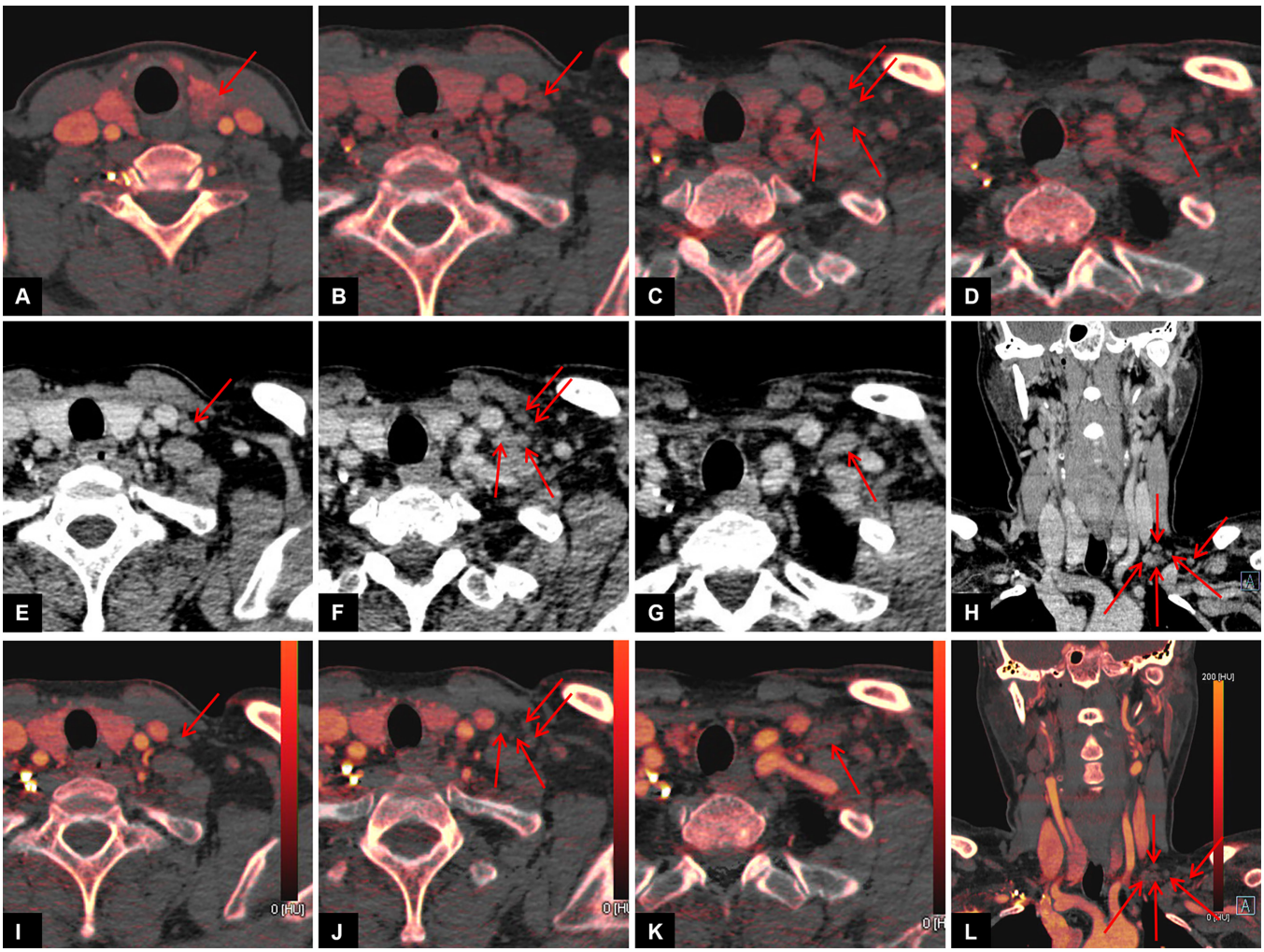

Figure S6. An example of pathological results and DECT both showing that all benign lymph nodes were in one level. Female, 48 years old, left lobe of the thyroid and left level VI dissection was performed. Pathology confirmed PTC of the left lobe with a diameter 2.0 cm (A) no metastatic LNs in the left level VIb were found among six dissected LNs. From the DECT images, we found six LNs in the left level VIb, and all were considered benign (B-D) iodine map in the arterial phase and on contrast-enhanced arterial phase (E-H). The ICs of these LNs were 2.2, 1.4, 2.1, 1.9, 2.4, and 1.8 mg/mL, respectively. In the venous phase, the ICs of these six metastatic LNs were 2.0, 1.4, 1.8, 1.7, 2.1, and 1.7 mg/mL, respectively (I-L). DECT, dual-energy computed tomography; IC, iodine concentration; PTC, papillary thyroid carcinoma; LN, lymph node.

http://dx.doi.org/10.21037/qims-20-846

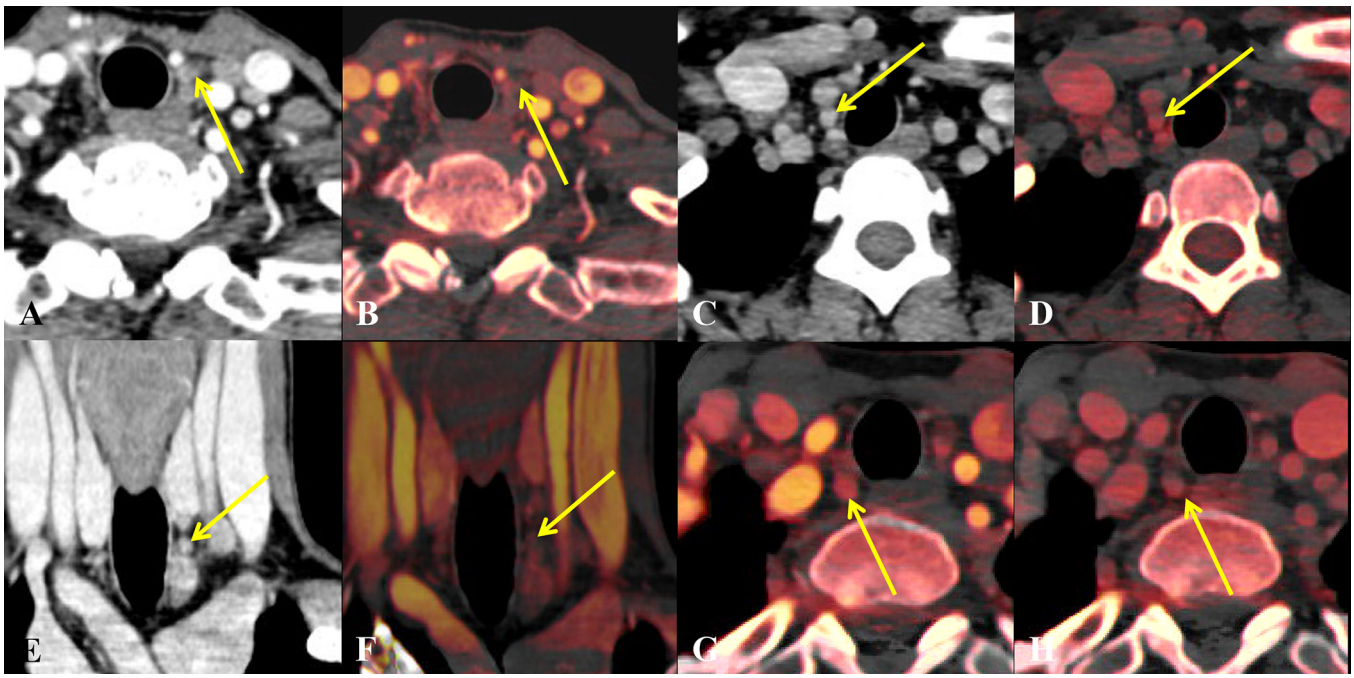

Figure S7 Illustration of the specific criteria for DECT to diagnose metastatic LNs. (A,B) A metastatic LN with cystic degeneration and heterogeneous enhancement in the left level VIb. (C,D) A metastatic LN with strong enhancement in the right level VIb. (E,F) A metastatic LN with micro-calcification in the left level VIb. (G,H) A metastatic LN in the right level VIb with IC of 4.7 mg/mL in the arterial phase, and 3.7 mg/mL in the venous phase. DECT, dual-energy computed tomography; IC, iodine concentration; LN, lymph node.

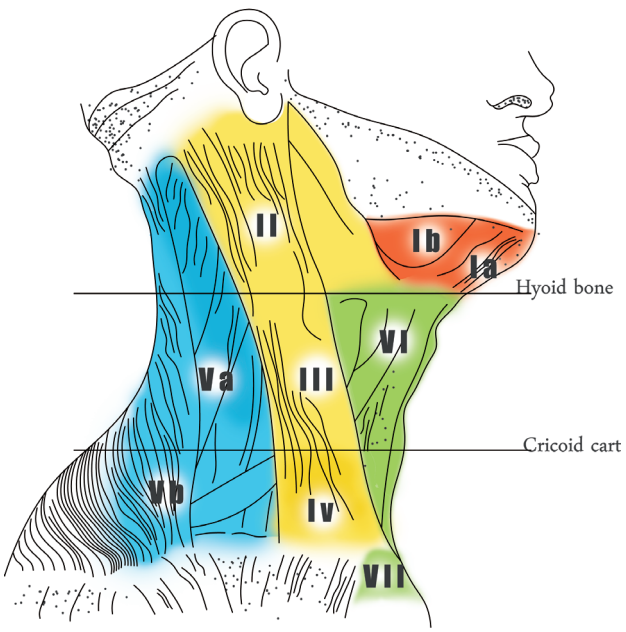

Figure S8 Schematic diagram of cervical LN division. LN, lymph node.

http://dx.doi.org/10.21037/qims-20-846

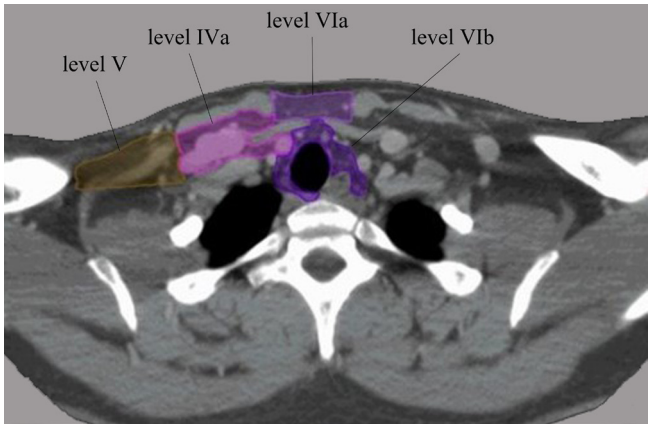

Figure S9 The boundaries of levels VIa and VIb. Level VI contains the anterior compartment nodes including superficially, the anterior jugular nodes (level VIa), and in the deep pre-visceral space, the pre-laryngeal, pre-tracheal, and para-tracheal (recurrent laryngeal nerve) nodes (level VIb). Level VIb receives efferent lymphatics from the anterior floor of the mouth, the tip of the tongue, the lower lip, the thyroid gland, the glottic and subglottic larynx, the hypopharynx, and the cervical esophagus. These nodes are at high risk of metastasis from cancers of the lower lip, the oral cavity, the thyroid gland, the glottic and subglottic larynx, the apex of the piriform sinus, and the cervical esophagus.

Table S1 Demographic, clinical, and pathological characteristics of participants

Characteristic	Statistical data
No. of patients	52
Sex, n (%)	
Male	11 (21.2)
Female	41 (78.8)
Age, years	44.3±11.4
Pathological type, n (%)	
PTC	36 (41.9)
PTMC	50 (58.1)
Multiple, n (%)	
Single	30 (57.7)
Multiple	22 (42.3)
Location, n (%)	
Left lobe	35 (40.7)
Right lobe	42 (48.8)
Isthmus	9 (10.5)
No. of subregions of LNs, n (%)	
Non-metastatic	101 (52.9)
Metastatic	90 (47.1)
No. of LNs, n (%)	
Non-metastatic	220 (61.3)
Metastatic	139 (38.7)

PTC, papillary thyroid carcinoma; PTMC, papillary thyroid microcarcinoma; LNs, lymph nodes.

Table S2 The boundaries of level VIa and VIb

Boundaries	Level VIa	Level VIb
Anterior	Skin or platysma muscle	Posterior aspect of infrahyoid muscle
Posterior	Anterior aspect of the infrahyoid muscle	Anterior aspect of the larynx, thyroid gland, and trachea
Cranial	Caudal edge of the hyoid bone or the submandibular gland	Caudal edge of the thyroid cartilage
Caudal	Cranial edge of the sternal manubrium	Cranial edge of the sternal manubrium
Lateral	Anterior edges of both sternocleidomastoid muscles	Common carotid artery on both sides
Medial	N/A	Lateral aspect of the trachea and esophagus

http://dx.doi.org/10.21037/qims-20-846

Table S3 Consistency analysis of the measurement parameters of the two radiologists

Parameters	ICC (95% CI)	P value
Diameter		
Doctor A	0.957 (0.921–0.976)	<0.001
Doctor B	0.958 (0.927–0.976)	<0.001
Doctor A and Doctor B	0.959 (0.919–0.978)	<0.001
IC in the arterial phase		
Doctor A	0.957 (0.925–0.975)	<0.001
Doctor B	0.958 (0.927–0.976)	<0.001
Doctor A and Doctor B	0.945 (0.657–0.981)	<0.001
IC in the venous phase		
Doctor A	0.984 (0.972–0.991)	<0.001
Doctor B	0.984 (0.972–0.991)	<0.001
Doctor A and Doctor B	0.978 (0.430–0.994)	<0.001

IC, iodine concentration; ICC, intraclass correlation coefficient; CI, confidence interval.

Table S5 Multicollinearity assessment in the prediction model based on the independent predictors

Predictors	Collinearity Statistics	
	Tolerance	VIF
Level	0.966	1.035
Diameter	0.981	1.019
ICIAP	0.762	1.313
ICIVP	0.790	1.265

VIF, variance inflation factor; ICIAP, iodine concentration in the arterial phase; ICIVP, iodine concentration in the venous phase.

Table S4 The differences among the AUCs of quantitative parameters

	DBA	95% CI	0.100	Z	P value
IC IAP *vs.* IC IVP	0.0216	−0.0396 to 0.0828		0.691	0.4895
IC IAP *vs.* NIC IAP	0.0151	−0.0146 to 0.0448		0.995	0.3198
IC IAP *vs.* NIC IVP	0.0241	−0.0402 to 0.0885		0.735	0.4622
IC IAP *vs.* λ_{HU} IAP	0.0974	0.042 to 0.153		3.451	0.0006
IC IAP *vs.* λ_{HU} IVP	0.165	0.0934 to 0.237		4.52	<0.0001
IC IVP *vs.* NIC IAP	0.00652	−0.0563 to 0.0694		0.203	0.8388
IC IVP *vs.* NIC IVP	0.00253	−0.0294 to 0.0344		0.156	0.8763
IC IVP *vs.* λ_{HU} IAP	0.0758	0.00766 to 0.144		2.18	0.0292
IC IVP *vs.* λ_{HU} IVP	0.143	0.0854 to 0.201		4.847	<0.0001
NIC IAP *vs.* NIC IVP	0.00906	−0.0511 to 0.0692		0.295	0.768
NIC IAP *vs.* λ_{HU} IAP	0.0823	0.0215 to 0.143		2.651	0.008
NIC IAP *vs.* λ_{HU} IVP	0.15	0.0745 to 0.225		3.899	0.0001
NIC IVP *vs.* λ_{HU} IAP	0.0733	0.00347 to 0.143		2.057	0.0396
NIC IVP *vs.* λ_{HU} IVP	0.141	0.0753 to 0.206		4.21	<0.0001
λ_{HU} IAP *vs.* λ_{HU} IVP	0.0676	0.00629 to 0.129		2.161	0.0307

AUC, area under the curve; CI, confidence interval; DBA, difference between areas; IC, iodine concentration; NIC, normalized iodine concentration; λ_{HU}, the slope of energy spectrum curve; IAP, in the arterial phase; IVP, in the venous phase.

http://dx.doi.org/10.21037/qims-20-846

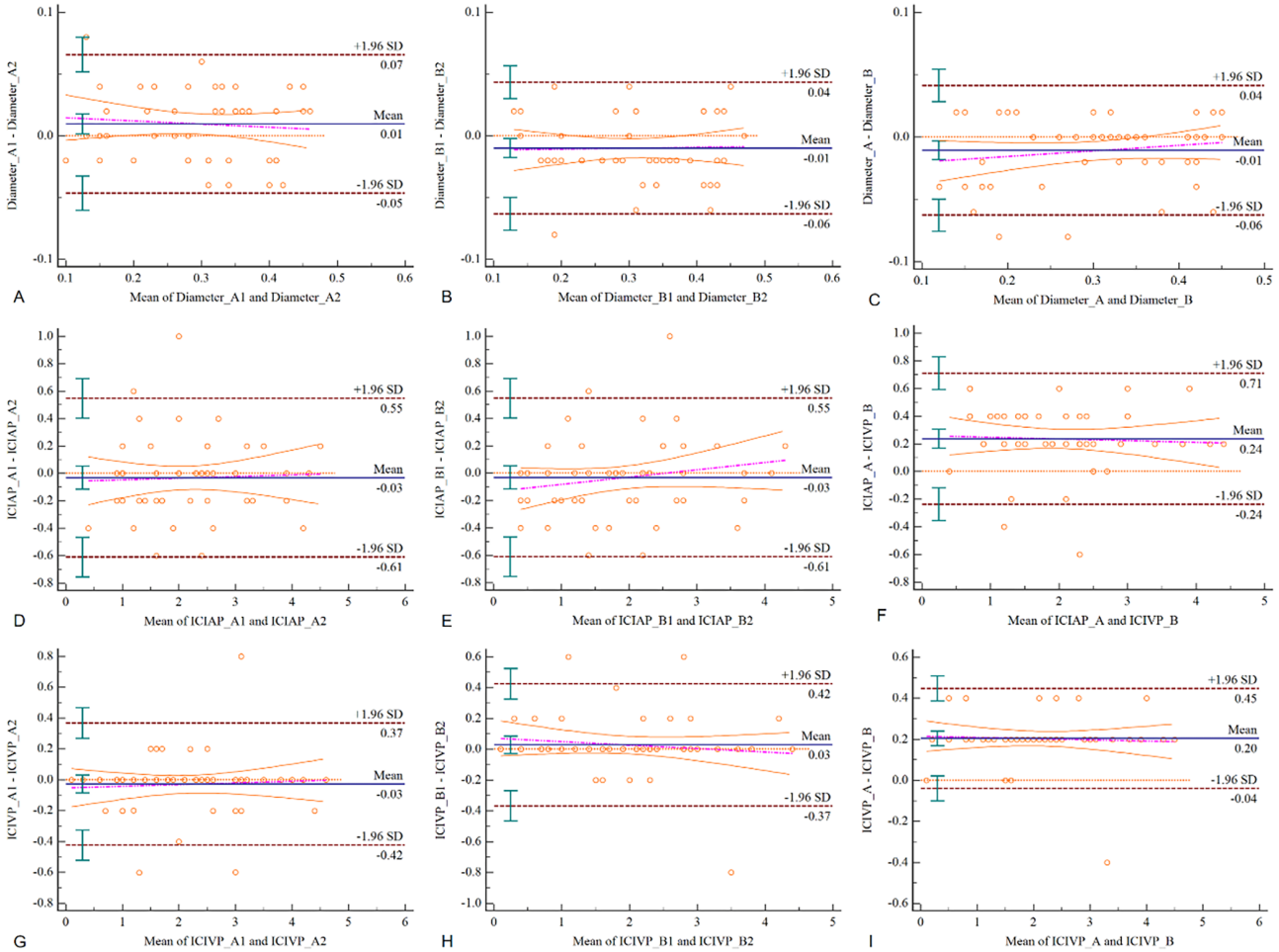

Figure S10 The inter- and intra-observer consistency analyses. The inter-observer consistency analysis result for the ICC of the diameter diagnostic test between doctor A and doctor B was 0.959 (P<0.001), and the intra-observer consistency analysis result for the diameter was 0.957 (P<0.001) and 0.958 (P<0.001) for doctor A and doctor B, respectively (A-C). The inter-observer consistency analysis result for the ICC of the IC in the arterial phase diagnostic test between doctor A and doctor B was 0.945 (P<0.001), and the intra-observer consistency analysis result for the IC in the arterial phase was 0.957 (P<0.001) and 0.958 (P<0.001) for doctor A and doctor B, respectively (D-F). The inter-observer consistency analysis result for the ICC of the IC in the venous phase diagnostic test between doctor A and doctor B was 0.978 (P<0.001), and the intra-observer consistency analysis result for the IC in the venous phase was 0.984 (P<0.001) and 0.984 (P<0.001) for doctor A and doctor B, respectively (G-I). ICC, intraclass correlation coefficient; IC, iodine concentration.

http://dx.doi.org/10.21037/qims-20-846

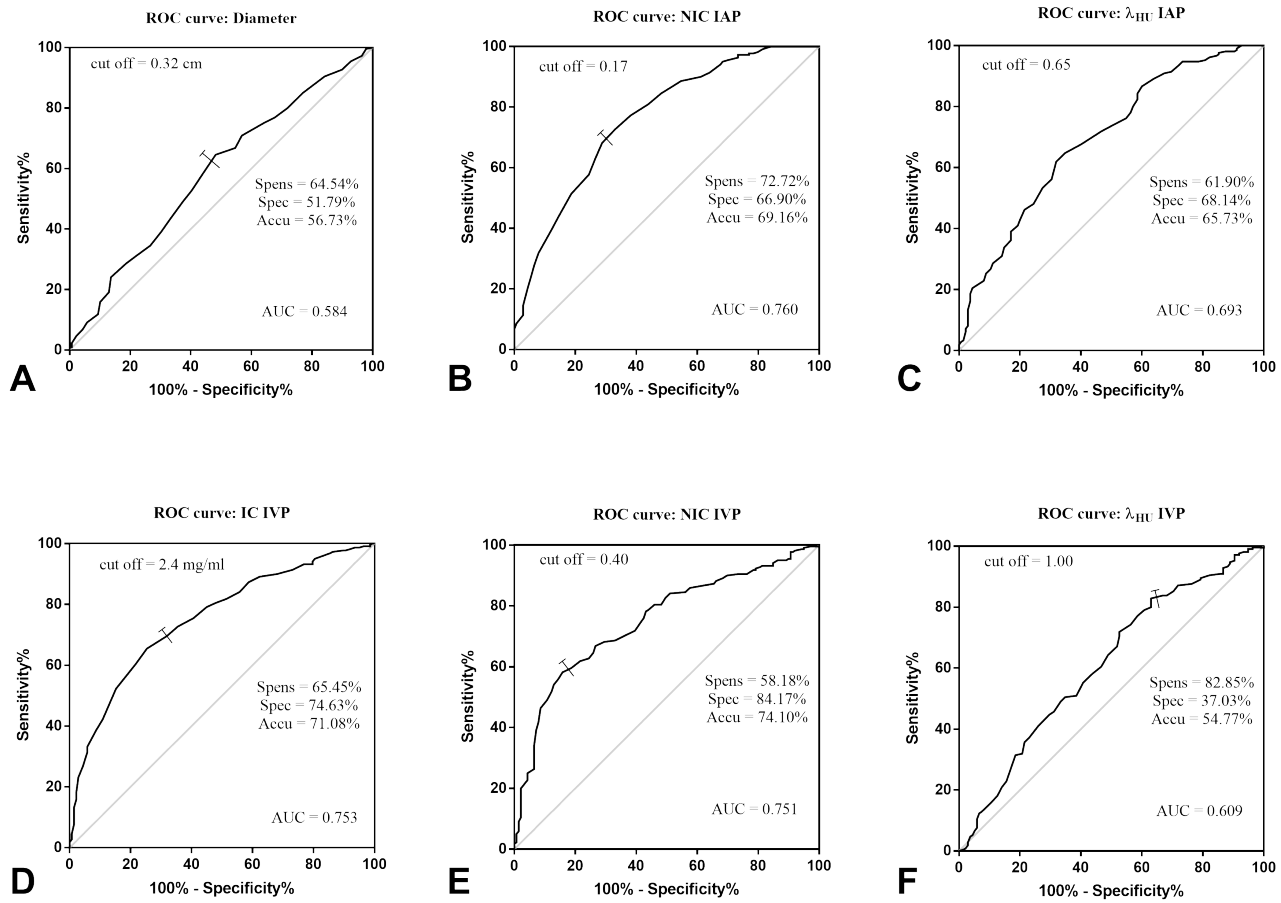

Figure S11 The ROC curves of the quantitative parameters derived from DECT. (A) The AUC, sensitivity, specificity, and accuracy of diameter were 0.584, 64.54%, 51.79%, and 56.73%, respectively, with a cut-off value of 0.32 cm. (B) The AUC, sensitivity, specificity, and accuracy of NIC in the arterial phase were 0.760, 72.72%, 66.90%, and 69.16%, respectively, with a cut-off value of 0.17. (C) The AUC, sensitivity, specificity, and accuracy of λ_{HU} in the arterial phase were 0.693, 61.90%, 68.14%, and 65.73%, respectively, with a cut-off value of 0.65. (D) The AUC, sensitivity, specificity, and accuracy of IC in the venous phase were 0.753, 65.45%, 74.63%, and 71.08%, respectively, with a cut-off value of 2.4 mg/mL. (E) The AUC, sensitivity, specificity, and accuracy of NIC in the venous phase were 0.751, 58.18%, 84.17%, and 74.10%, respectively, with a cut-off value of 0.40. (F) The AUC, sensitivity, specificity, and accuracy of λ_{HU} in the venous phase were 0.609, 82.85%, 37.03%, and 54.77%, respectively, with a cut-off value of 1.00. ROC, receiver operating characteristic; NIC, normalized iodine concentration; IAP, in the arterial phase; λ_{HU}, the slope of energy spectrum curve; IC, iodine concentration; IVP, in the venous phase; DECT, dual-energy computed tomography; AUC, area under the curve

http://dx.doi.org/10.21037/qims-20-846

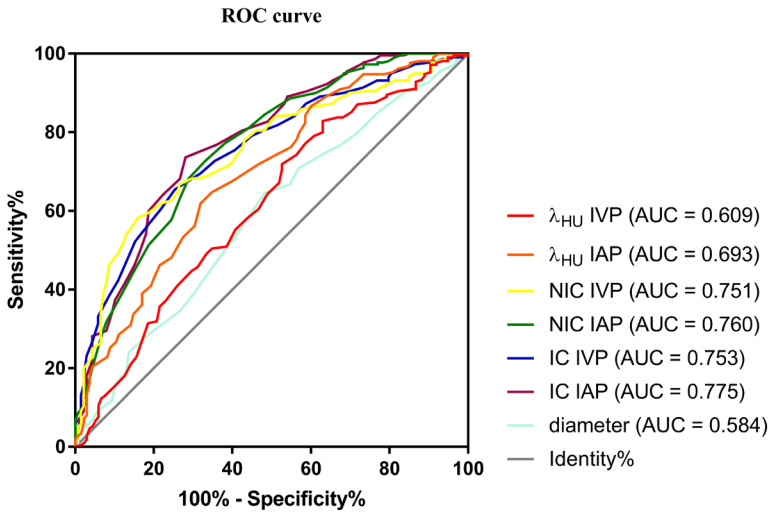

Figure S12 The mixed ROC curves of the quantitative parameters derived from DECT. The AUC was a global measure of the ability of a test to discriminate whether a specific condition was present or not present. An AUC of 0.5 represented a test with no discrimination, while an AUC of 1.0 represented a test with perfect discrimination. The AUCs of diameter, IC IAP, IC IVP, NIC IAP, NIC IVP, λ_{HU} IAP, and λ_{HU} IVP were 0.584, 0.775, 0.753, 0.760, 0.751, 0.693, and 0.609, respectively. Among them, IC IAP had the highest AUC, indicating that it was the most significant for the differentiation of metastatic and non-metastatic LNs. ROC, receiver operating characteristic; DECT, dual-energy computed tomography; AUC, area under the curve; IC, iodine concentration; IAP, in the arterial phase; IVP, in the venous phase; NIC, normalized iodine concentration; λ_{HU}, the slope of energy spectrum curve; LNs, lymph nodes.

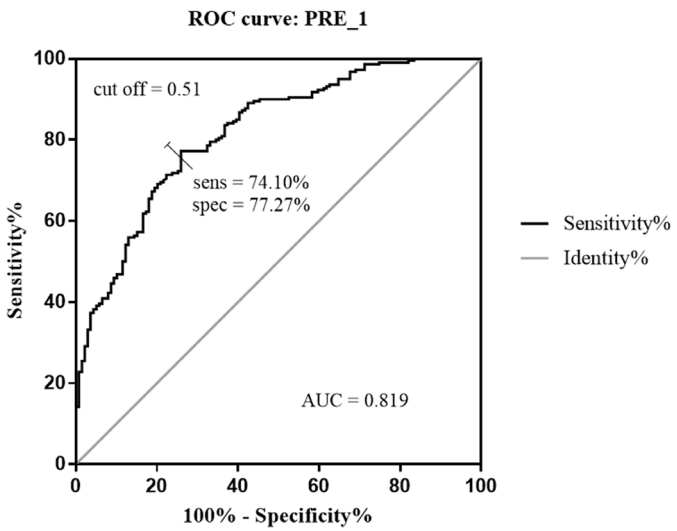

Figure S13 The ROC curve of three combined parameters (diameter, IC in the arterial phase, and NIC in the venous phase) was used to identify metastatic and non-metastatic lymph nodes. When the cut-off value with 0.51, the sensitivity, and specificity were 74.10%, and 77.27%, respectively. The 95% CI: was 0.776–0.858. PRE, prediction probability; ROC, receiver operating characteristic; IC, iodine concentration; NIC, normalized iodine concentration; AUC, area under the curve; CI, confidence interval.

http://dx.doi.org/10.21037/qims-20-846

diagnosis of thyroid cancer, we simply did not repeat them here. In addition to the relevant literature, we also consulted the international and domestic guidelines on thyroid cancer and extracted the relevant introductions about CT, which are described in detail below.

The American Thyroid Association (ATA) statement on preoperative imaging for thyroid cancer surgery (9) highlighted that contrast CT may be applied to evaluate lymphadenopathy fully when physical examination and/or US suggest bulky or extensive nodal metastasis is unable to be completely evaluated with US. The statement emphasized that the combination of CT with US in preoperative lymph node evaluation is superior to the use of either modality alone.

In the Chinese Society of Clinical Oncology (CSCO) diagnosis and treatment guidelines for persistent/recurrent and metastatic differentiated thyroid cancer (version 2018) (56), when there are suspected local lesions, enhanced CT is juxtaposed as a level I–2A recommendation.

In the National Comprehensive Cancer Network (NCCN) guidelines (version 2018) (33), for papillary carcinoma or suspicious for papillary carcinoma, the use of CT with contrast was suggested for fixed, bulky, or substernal lesions. The NCCN guidelines (2020 V1) for diagnosing papillary carcinoma or suspected papillary carcinoma recommend the use of CT with contrast for locally advanced disease or vocal cord paresis.

The evidence provided in the above guidelines support the idea that enhanced CT is not a contraindication for patients with PTC. Moreover, CT examination can more accurately determine the extent of LNM, which is essential in the planning of surgical procedures.

In the current study, the patients were first suspected to have a malignant thyroid lesion with LNM by US, which was later confirmed as PTC by US-guided fine-needle aspiration biopsy (US-FNAB). DECT was performed to rule out or confirm the presence of LNM (45).

We used DECT for preoperative imaging instead of traditional enhanced CT due to its many advantages in comparison. The reasons for using DECT in the current study were as follows. First, its radiation dose (total dose-length product, DLP) was 5–6 times lower than that of ordinary enhanced CT (57). Second, DECT achieves a better image quality with significantly lower kVp and tube current. Third, DECT realizes multi-parameter imaging, such as single-energy images, energy spectrum curves, base material images, and the quantitative concentration values and effective atomic numbers of corresponding base materials. The biggest advantage of DECT is that it not only shows morphological changes, but it also provides many quantitative indicators that could reflect the essential characteristics of lesions (58). The current study applied DECT to predict cervical metastatic lymph nodes with a diameter <0.5 cm in patients with PTC preoperatively, and to guide the planning of clinical procedures, which has not been reported before.

Preoperative DECT did not delay radioiodine ablation in patients with PTC

The NCCN guidelines (version 2018 and version 2020 V1) (19,20) clearly state that iodinated contrast is required for optimal cervical imaging using CT and that a delay in RAI treatment is not harmful to the patient.

Yeh *et al*. researched the content "Use of Iodinated Contrast and Impact on Subsequent Treatment" (9). The results showed that CT imaging of the neck was optimized by iodinated intravenous contrast. This advantage had to be balanced against the impact the iodine load would have in causing what was usually a minor delay in subsequent postoperative RAI ablation. After the administration of iodinated contrast, a waiting period of ≥1 month was recommended to allow urinary iodine levels to return to baseline levels before proceeding with RAI ablation (59). The CSCO expert consensus on the evaluation of ^{131}I before the treatment of differentiated thyroid cancer gave similar guidance. At present, there is no evidence to suggest that delays of this scale adversely affect thyroid cancer outcomes.

As we know, >90% of administered iodine is excreted in urine, and as the thyroid is the major reservoir of iodine in the body, iodine content should fall rapidly after total thyroidectomy, even in patients undergoing preoperative DECT (60). Furthermore, the recommendations against performing contrast-enhanced CT seem to be based on studies conducted in the past when lipophilic contrast agents were in use, which tend to be stored in adipose tissues for a long time. Currently the majority of centers use water-soluble ionic contrast agents (such as iohexol, which was used in our study), which are unlikely to be retained in extracellular fluids (60). Therefore, unless there is further iodine contamination, the UIC should soon revert to the previous equilibrium after DECT examination. Many studies have reported the time for UIC to normalize to be between 30 and 43 days (59-62). In addition, in routine practice, if the patients with PTC who come to our hospital for surgery need postoperative RAI therapy, the whole process "preoperative examination → thyroidectomy →

http://dx.doi.org/10.21037/qims-20-846

postoperative rehabilitation and discharge → appointment and preparation before RAI therapy → admission for RAI therapy" need to be completed. The entire process took ≥6 weeks without any delay, which was longer than required in the ATA guidelines. The 2015 ATA guidelines stated that postoperative RAI therapy should be routinely administered only to patients with high-risk differentiated thyroid cancer (DTC); it is not recommended for low-risk DTC and should only be considered for patients in the ATA intermediate-risk group (63). The majority of studies showed that the timing of post-thyroidectomy initial RAI therapy did not affect the OS or long-term outcomes of patients (64-68). Therefore, RAI administration may be safely planned according to the logistics of the local health administration and the individual patient (64).

In the current study, all participants who underwent DECT examination before surgery were given ≥1 month to recover before undergoing ^{131}I treatment after surgery, and the delay did not cause any harm according to our follow-up results.

Other inclusion criteria

Contrast agent enhancement of DECT depends on two factors. Firstly, injection-related factors, including contrast agent concentration and injection volume, contrast agent type, and saline injection; and secondly, patient-related factors, including cardiac output and BMI (69,70). Therefore, in the current study, we included participants with normal BMI (18.5–24.9 kg/m^2). Overweight patients have decreased arterial enhancement. There is a negative linear relationship between body weight and the CT value of the common carotid artery (71). In addition, there is a moderate negative correlation between height and the CT value of the aorta (72). Since height is proportional to weight, the effect of height and weight on arterial strengthening should be in the same direction, and the effect of height should be weaker than that of weight. To eliminate the effect of different heights on weight and to enable a clearer comparison between groups in this study, patients with a normal BMI were selected.

Specific DECT diagnostic criteria of metastatic lymph nodes <0.5 cm in patients with PTC

Based on the previous CT diagnostic criteria for metastatic LNs, DECT diagnostic methods, and our clinical imaging diagnosis experience, we summarized the following criteria for diagnosing LNM with a diameter <0.5 cm: strong or heterogeneous enhancement; micro-calcification; cystic degeneration or necrosis; extranodal extension; IC in the arterial phase ≥2.1 mg/mL; and IC in the venous phase ≥2.4 mg/mL (18,34,36) (*Figure S7*). Strong enhancement was considered to be similar to that of the pharyngeal mucosa. Fuzzy boundaries and/or invasion into adjacent tissues were considered to indicate extranodal extension (34).

DECT examination

Patients were instructed to hold their breath during eupnea before the horizontal scan in a transverse position. All patients were scanned craniocaudally in the supine position with the bilateral upper limbs placed on both sides, shoulders drooping maximally, and head slightly tilted. The longitudinal alignment of the positioning cursor was on the central sagittal plane of the cervicothoracic region. The orthotopic scanning was performed first, and then the scanning baseline and range were confirmed according to the scout view. The whole neck was scanned from the upper edge of the aortic arch to the lower edge of the submandibular gland, which covered the area of the thyroid and cervical lymph nodes.

The patient's heart rate was maintained at a normal level throughout the scan. After CT scanning, arterial phase and venous phase contrast-enhanced scanning was performed. The images were acquired in the dual-energy mode using the following parameters: tube current, 600 mA; helical thickness, 6 mm; helical pitch, 0.9; rotation speed, 0.28 s; detector width, 40 mm; collimation, 64 mm × 0.6 mm. The scanning parameters were set according to the concept of as low as reasonably achievable for radiation protection. A fast rotation speed and a moderate helical pitch were chosen to obtain fast scanning speed and reduce motion artifacts of neck and radiation dose. For contrast-enhanced scanning, an iodinated nonionic contrast agent (iohexol; 350 mg/dL iodine, Somatom Definition Flash, Siemens Healthcare, Forchheim, Germany) was administered through the right elbow median vein by a dual-head injector. The dosage was 1 mL/kg with a flow rate of 3 mL/s, the total injection dose was 60–70 mL, followed by a bolus injection of 40 mL saline given at the same flow rate. The timing of arterial phase scanning was determined by automatic trigger technique. The scanning delay at the beginning of arterial phase scanning was 25 s. After the arterial scan had been completed, the scanning delay time of the venous scan was 20 s.

http://dx.doi.org/10.21037/qims-20-846

All the original CT data were reconstructed into contiguous axial images with a section thickness of 1 mm, a field of view (FOV) of 200 mm and a matrix of 512×512. The DECT data of arterial and venous phases were transferred to Siemens syngo.via workstation (Syngo DE, Siemens Healthcare, Forchheim, Germany) for analysis, the Liver VNC function keys for computer automatic processing, then the iodine maps were obtained.

Criteria for region of interest (ROI) selection in the current study

Firstly, under the premise of ensuring a clear image, we zoomed in to accurately measure the lesion. Secondly, we referred to the enhanced images of the arterial and venous phases and the iodine maps of the arterial and venous phases, and selected the layer that can clearly and completely display the largest cross-sectional area of the lymph node. Combining the sagittal, coronal, and axial images, the lymph node with the largest cross-sectional area for measurement was selected. The ROI was placed on the largest possible solid part, with attention paid to avoid cystic degeneration, necrosis, or calcification, and not involve adjacent blood vessels.

The division of cervical lymph nodes (focus on VIb)

In the American Joint Committee on Cancer (AJCC) 8th edition guidelines, the division of cervical lymph nodes plays an important role in clinical diagnosis and treatment. It meets the needs of the otolaryngology, head and neck surgery, and radiotherapy departments for the accurate positioning of cervical lymph nodes, as well as regulating the examination and facilitating academic exchange. However, it does not clearly define the parotid gland, cheeks, or scalp lymph node drainage, and some of the anatomical boundaries are not very accurate. In November 2013, the official journal of the European Society of Radiotherapy & Oncology (ESTRO)-Radiotherapy & Oncology (Green Skin Magazine) published a new cervical lymph node partition standard, which stated that according to the knowledge of anatomy, surgery, and imaging, the boundary should be accurately integrated into the axial CT image as much as possible. And the standard CT image was divided level VI into VIa and VIb (36). This is the most recently published cervical lymph node partition standard (*Table S2*, *Figures S8*,*S9*).

Result of consistency analysis

The inter-observer consistency analysis result for the ICC of the diameter diagnostic test between doctor A and doctor B was 0.959 ($P<0.001$) and the intra-observer consistency analysis result for the diameter was 0.957 ($P<0.001$) and 0.958 ($P<0.001$) for doctor A and doctor B, respectively. The inter-observer consistency analysis result for ICC of the IC in the arterial phase diagnostic test between doctor A and doctor B was 0.945 ($P<0.001$) and intra-observer consistency analysis result for the IC in the arterial phase was 0.957 ($P<0.001$), and 0.958 ($P<0.001$) respectively in doctor A and doctor B, respectively. The inter-observer consistency analysis result for ICC of the IC in venous phase diagnostic testing between doctor A and doctor B was 0.978 ($P<0.001$), and intra-observer consistency analysis result for the IC in the venous phase was 0.984 ($P<0.001$), and 0.984 ($P<0.001$), respectively.

References

43. Suh CH, Baek JH, Choi YJ, Lee JH. Performance of CT in the Preoperative Diagnosis of Cervical Lymph Node Metastasis in Patients with Papillary Thyroid Cancer: A Systematic Review and Meta-Analysis. AJNR Am J Neuroradiol 2017;38:154-61.
44. Lee Y, Kim JH, Baek JH, Jung SL, Park SW, Kim J, Yun TJ, Ha EJ, Lee KE, Kwon SY, Yang K S, Na DG. Value of CT added to ultrasonography for the diagnosis of lymph node metastasis in patients with thyroid cancer. Head Neck 2018;40:2137-48.
45. Cho SJ, Suh CH, Baek JH, Chung SR, Choi YJ, Lee JH. Diagnostic performance of CT in detection of metastatic cervical lymph nodes in patients with thyroid cancer: a systematic review and meta-analysis. Eur Radiol 2019;29:4635-47.
46. He M, Lin C, Yin L, Lin Y, Zhang S, Ma M. Value of Dual-Energy Computed Tomography for Diagnosing Cervical Lymph Node Metastasis in Patients With Papillary Thyroid Cancer. J Comput Assist Tomogr 2019;43:970-5.
47. Hong D, Lee S, Kim T, Baek JH, Lee YM, Chung KW, Sung TY, Kim N. Development of a personalized and realistic educational thyroid cancer phantom based on CT images: An evaluation of accuracy between three different 3D printers. Comput Biol Med 2019;113:103393.
48. Lee DH, Lee YH, Seo HS, Lee KY, Suh SI, Ryoo I,

http://dx.doi.org/10.21037/qims-20-846

You SH, Kim B, Yang KS. Dual-energy CT iodine quantification for characterizing focal thyroid lesions. Head Neck 2019;41:1024-31.
49. Lee JH, Ha EJ, Kim JH. Application of deep learning to the diagnosis of cervical lymph node metastasis from thyroid cancer with CT. Eur Radiol 2019;29:5452-7.
50. Yeom JA, Roh J, Jeong YJ, Lee JC, Kim HY, Suh YJ, Baik SK. Ultra-Low-Dose Neck CT With Low-Dose Contrast Material for Preoperative Staging of Thyroid Cancer: Image Quality and Diagnostic Performance. AJR Am J Roentgenol 2019;212:748-54.
51. Debnam JM, Guha-Thakurta N, Sun J, Wei W, Zafereo ME, Cabanillas ME, Buisson NM, Schellingerhout D. Distinguishing Recurrent Thyroid Cancer from Residual Nonmalignant Thyroid Tissue Using Multiphasic Multidetector CT. AJNR Am J Neuroradiol 2020;41:844-51.
52. Wei P, Jiang N, Ding J, Xiang J, Wang L, Wang H, Gu Y, Luo D, Han Z. The Diagnostic Role of Computed Tomography for ACR TI-RADS 4-5 Thyroid Nodules With Coarse Calcifications. Front Oncol 2020;10:911.
53. Wei PY, Jiang ND, Xiang JJ, Xu CK, Ding JW, Wang HB, Luo DC, Han ZJ. Hounsfield Unit Values in ACR TI-RADS 4-5 Thyroid Nodules with Coarse Calcifications: An Important Imaging Feature Helpful for Diagnosis. Cancer Manag Res 2020;12:2711-7.
54. Xing Z, Qiu Y, Yang Q, Yu Y, Liu J, Fei Y, Su A, Zhu J. Thyroid cancer neck lymph nodes metastasis: Meta-analysis of US and CT diagnosis. Eur J Radiol 2020;129:109103.
55. Zhou Y, Su GY, Hu H, Ge YQ, Si Y, Shen MP, Xu XQ, Wu FY. Radiomics analysis of dual-energy CT-derived iodine maps for diagnosing metastatic cervical lymph nodes in patients with papillary thyroid cancer. Eur Radiol 2020;30:6251-62.
56. Chinese Society of Clinical Oncology (CSCO) diagnosis and treatment guidelines for persistent/recurrent and metastatic differentiated thyroid cancer 2018 (English version). Chin J Cancer Res 2019;31:99-116.
57. Agostini A, Mari A, Lanza C, Schicchi N, Borgheresi A, Maggi S, Giovagnoni A. Trends in radiation dose and image quality for pediatric patients with a multidetector CT and a third-generation dual-source dual-energy CT. Radiol Med 2019;124:745-52.
58. Ren L, Rajendran K, McCollough CH, Yu L. Quantitative accuracy and dose efficiency of dual-contrast imaging using dual-energy CT: a phantom study. Med Phy 2020;47:441-56.
59. Padovani RP, Kasamatsu TS, Nakabashi CC, Camacho CP, Andreoni DM, Malouf EZ, Marone MM, Maciel RM, Biscolla RP. One month is sufficient for urinary iodine to return to its baseline value after the use of water-soluble iodinated contrast agents in post-thyroidectomy patients requiring radioiodine therapy. Thyroid 2012;22:926-30.
60. Mishra A, Pradhan PK, Gambhir S, Sabaretnam M, Gupta A, Babu S. Preoperative contrast-enhanced computerized tomography should not delay radioiodine ablation in differentiated thyroid carcinoma patients. J Surg Res 2015;193:731-7.
61. Nimmons GL, Funk GF, Graham MM, Pagedar NA. Urinary iodine excretion after contrast computed tomography scan: implications for radioactive iodine use. JAMA Otolaryngol Head Neck Surg 2013;139:479-82.
62. Sohn SY, Choi JH, Kim NK, Joung JY, Cho YY, Park SM, Bae JC, Lee SY, Chung JH, Kim SW. The impact of iodinated contrast agent administered during preoperative computed tomography scan on body iodine pool in patients with differentiated thyroid cancer preparing for radioactive iodine treatment. Thyroid 2014;24:872-7.
63. Haugen BR, Alexander EK, Bible KC, Doherty GM, Mandel SJ, Nikiforov YE, Pacini F, Randolph GW, Sawka AM, Schlumberger M, Schuff KG, Sherman SI, Sosa JA, Steward DL, Tuttle RM, Wartofsky L. 2015 American Thyroid Association Management Guidelines for Adult Patients with Thyroid Nodules and Differentiated Thyroid Cancer: The American Thyroid Association Guidelines Task Force on Thyroid Nodules and Differentiated Thyroid Cancer. Thyroid 2016;26:1-133.
64. Suman P, Wang CH, Moo-Young TA, Prinz RA, DJ W. Timing of radioactive iodine administration does not influence outcomes in patients with differentiated thyroid carcinoma. Thyroid 2016;26:1623-9.
65. Tsirona S, Vlassopoulou V, Tzanela M, Rondogianni P, Ioannidis G, Vassilopoulos C, Botoula E, Trivizas P, Datseris I, Tsagarakis S. Impact of early vs late postoperative radioiodine remnant ablation on final outcome in patients with low-risk well-differentiated thyroid cancer. Clin Endocrinol (Oxf) 2014;80:459-63.
66. Krajewska J, Jarzab M, Kukulska A, Czarniecka A, Roskosz J, Puch Z, Wygoda Z, Paliczka-Cieslik E, Kropinska A, Krol A, Handkiewicz-Junak D, Jarzab B. Postoperative Radioiodine Treatment within 9 Months from Diagnosis Significantly Reduces the Risk of Relapse in Low-Risk Differentiated Thyroid Carcinoma. Nucl Med Mol Imaging 2019;53:320-7.
67. Kim M, Han M, Jeon MJ, Kim WG, Kim IJ, Ryu JS, Kim

http://dx.doi.org/10.21037/qims-20-846

WB, Shong YK, Kim TY, Kim BH. Impact of delayed radioiodine therapy in intermediate-/high-risk papillary thyroid carcinoma. Clin Endocrinol (Oxf) 2019;91:449-55.
68. Suman P, Wang CH, Abadin SS, Block R, Raghavan V, Moo-Young TA, Prinz RA, Winchester DJ. Timing of Radioactive Iodine Therapy Does Not Impact Overall Survival in High-Risk Papillary Thyroid Carcinoma. Endocr Pract 2016;22:822-31.
69. Schoellnast H, Deutschmann HA, Berghold A, Fritz GA, Schaffler GJ, Tillich M. MDCT angiography of the pulmonary arteries: influence of body weight, body mass index, and scan length on arterial enhancement at different iodine flow rates. AJR Am J Roentgenol 2006;187:1074-8.
70. Bae KT, Seeck BA, Hildebolt CF, Tao C, Zhu F, Kanematsu M, Woodard PK. Contrast enhancement in cardiovascular MDCT: effect of body weight, height, body surface area, body mass index, and obesity. AJR Am J Roentgenol 2008;190:777-84.
71. Bae KT, Tao C, Gurel S, Hong C, Zhu F, Gebke TA, Milite M, Hildebolt CF. Effect of patient weight and scanning duration on contrast enhancement during pulmonary multidetector CT angiography. Radiology 2007;242:582-9.
72. Awai K, Hori S. Effect of contrast injection protocol with dose tailored to patient weight and fixed injection duration on aortic and hepatic enhancement at multidetector-row helical CT. Eur Radiol 2003;13:2155-60.
73. Gregoire V, Ang K, Budach W, Grau C, Hamoir M, Langendijk JA, Lee A, Le QT, Maingon P, Nutting C, O'Sullivan B, Porceddu SV, Lengele B. Delineation of the neck node levels for head and neck tumors: a 2013 update. DAHANCA, EORTC, HKNPCSG, NCIC CTG, NCRI, RTOG, TROG consensus guidelines. Radiother Oncol 2014;110:172-81.

http://dx.doi.org/10.21037/qims-20-846